Estimation of thermal residual stresses in HA-glass functionally graded bio-coating

Proceedings of the Seventeenth (2007) International Offshore and Polar Engineering Conference
Lisbon, Portugal, July 1-6, 2007

ISBN 978-1-880653-68-5; ISBN 1-880653-68-0(Set); ISSN 1098-6189 (Set)

Estimation of Thermal Residual Stresses in HA-glass Functionally Graded Bio-coating

Yukio Hirose[1], Lei Che*[2], Masahide Gotoh*[3], Lin Yang*[4]*
*1 Kanazawa University, Kanazawa, Ishikawa, JAPAN
*2 Graduate Student, Kanazawa University, Kanazawa, Ishikawa, JAPAN
*3 VBL, Kanazawa University, Kanazawa, Ishikawa, JAPAN
*4 Dalian Institute of Light Industry, Dalian, Liaoning, CHINA

ABSTRACT

Hydroxyapatite (HA) coatings have been widely used to provide a biocompatible surface on the dental and prosthetic implants. To improve the mechanical strength of the coating, we choose HA-glass functionally graded materials as coating materials. The functionally graded structure has been proved to be able to mitigate the residual stresses in materials near the interface of the coating and the substrate. The residual stresses are mainly caused by the mismatch in thermal expansions of the coating material and the substrate material. However, it is also a crucial requirement to evaluate the effect of the spatial distribution of constituent phases on the thermal residual stress distributions in the functionally graded coatings. With this aim, we measure the thermal residual states in the coatings by means of X-ray diffraction technique and simulate them using a computational model which applies the finite element method at the microscale. The experimental and the computational results show that the graded compound HA-glass interlayer structure can mitigate internal stresses and control the density and kinetics of misfit emanating from interfaces effectively.

KEY WORDS: Hydroxyapatite; Glass; Ceramic; Microstructure; Thermal residual stress; X-ray; FEM;

INTRODUCTION

Hydroxyapatite ceramic ($Ca_{10}(PO_4)_6(OH)_2$; HA) has been used successfully as a substitute material for defective bone issue because of its good osteointegration and biocompatibility. (Holmes, 1986; Klein, 1994) However, the HA material still cannot be used for implants under heavy loads directly due to its low tensile strength and low resistance to fatigue failure. (Brown, 1994) Using HA as a coating on metallic substrates is an innovation, which can compensate for the insufficient mechanical strength and maintain the biocompatibility of HA. (Geesink, 1987) Various coating techniques, such as plasma spraying, dip coating, hot isostatic pressing (HIP) and ion-beam sputtering, have been used successfully in coating HA on the metallic substrate. (Berndt, 1990; Li, 1996; Lacefield, 1988; Ong, 1994) Nevertheless, the previous studies (Wang, 1993; Yang, 2000) have demonstrated that, under the shear loading condition, the implants could fail in the bone near the HA coating-bone interface and at the HA coating-titanium alloy substrate interface. Residual stress that caused in the coating process is proposed to be one of the major reasons. After the coating processing, two kinds of stresses, "thermal stresses" and "intrinsic stresses", generate inevitably. Temperature excursions cause the "thermal stresses" due to expansion/contraction mismatch between the constituent phases in coatings or between the contiguous layers in the functionally graded coatings. Generation of the "intrinsic stresses" depends strongly on the processing methods and conditions used to deposit coatings on the substrates.

Functionally graded materials (FGMs) are an innovative class of composite materials. Their distinguishing characteristic is that the component phases are not uniformly distributed spatially. The spatial change in mechanical and thermal properties can be controlled through arranging compositional and microstructural gradient in the material. (Miyamoto, 1999) Therefore, we can use the gradient change in composition and microstructure of HA coating minimizes the residual thermal stresses which are caused by the heterogeneity of the coating material and the substrate material. To reduce the "intrinsic stresses" induced in the deposition process, slurry-dipping and sintering method is proved to be one available method for depositing functionally graded coatings on a ceramic substrate. (Che, 2007)

In this study, hydroxyapatite(HA)-glass functionally graded coating is deposited on the nanometer zirconia toughened alumina (ZTA) ceramic substrate using slurry-dipping and sintering method. To clarify the effect of microstructual discreteness on the actual thermal stress distribution in the coating, we estimated the residual stresses by means of X-ray diffraction technique and finite element method at the microscale. The results show that the graded interlayer structure can mitigate internal stresses and control the density and kinetics of misfit emanating from interfaces.

MATERIAL

Ingredient Materials

Materials used for the coating and the substrate are listed in Table 1. HA-glass functionally graded material was used as the coating material. As for the glass phase, a composition belonging to R_2O-Al_2O_3-B_2O_3-SiO_2 glass system, R_2O includes Na_2O and K_2O, was chosen. This system glass can effectively promote the sinterability of HA. (Wang, 2003) In order to reduce thermal coefficient difference between the

coating and the substrate, which may induce large residual stresses near the interface, a nanometer zirconia toughened alumina (ZTA) ceramic was used as the substrate material. Alumina (Al_2O_3) and zicornia (ZrO_2) are typical ceramics which have a good biocompatibility. It has been proved in previous study that the mechanical properties of alumina ceramics can be increased by incorporating 15wt.% ZrO_2. (Rao, 2003) Furthermore, thermal property of the ZTA ceramic is similar to that of the glass material (Table 2). Considering these reasons, ZTA ceramic plates, Φ15×3mm, were thus used as the substrates.

Table 1. Materials used for the coating and the substrate

	Material	Composition	Content (wt.%)	Size (μm)
Coating	Hydroxyapatite	$Ca_{10}(PO4)_6(OH)_2$	in Table 3	<75
	Wollastonite	$CaSiO_3$	in Table 3	<75
	Glass*1	R_2O-Al_2O_3-B_2O_3-SiO_2	in Table 3	<75
Substrate	Alumina	Al_2O_3	82	1
	Zirconia	ZrO_2	15	0.2
	Glass*2	CaO-MgO-Al_2O_3-SiO_2	3	10

Table 2. Materials properties (Grenoble, 1972; Borom, 1975)

Materials	Young modulus (GPa)	Poisson radio	Coefficient of thermal expansion ($\times 10^{-6}$ °C^{-1})
HA	114	0.28	12
Glass*1	102	0.26	10.4
Substrate	190	0.23	10

Functionally Graded Coating (FGC)

HA, $CaSiO_3$ and glass powders were dispersed into ethanol solution and homogenized by ultrasonic in order to prepare HA sols. Components of the composite powders used for sols were prepared as listed in Table 3. The FGC samples were coated on the ceramic substrate by means of Slurry-dripping and sintering method. The coating processing was as follows: the substrate plates were dipped into the HA sol (HA0-G9), and sintered under the air condition after being aired; the dip-sintered specimens were dipped into the second HA sol (e.g. HA1-G8), aired, and sintered subsequently. The same processes were repeated until the last layer was coated, as shown in Fig.2. Thickness of each coated layer was the same. After every slurry-dripping and sintering step, two specimens were reserved for stress measurements and microstructure observations. Thickness of the coating can be determined by the dipping-airing times. In this work, 150μm and 360μm, two kinds of coatings were prepared. Micrograph of the coating is shown in Fig.3.

Table 3. Components of the composite powders used for sols (wt.%)

	Number	HA	Glass	$CaSiO_3$
Layer1	HA0-G9	0	90	10
Layer2	HA1-G8	10	80	10
–	HA2-G7	20	70	10
Layer3	HA3-G6	30	60	10
–	HA4-G5	40	50	10
Layer4	HA5-G4	50	40	10
–	HA6-G8	60	30	10
Layer5	HA7-G2	70	20	10
–	HA8-G8	80	10	10
Layer6	HA9-G1	90	10	0
–	HA10	100	0	0

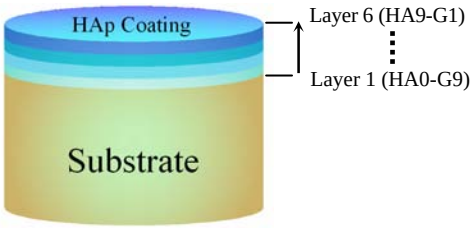

Figure.2 Image of a graded structure in the coating

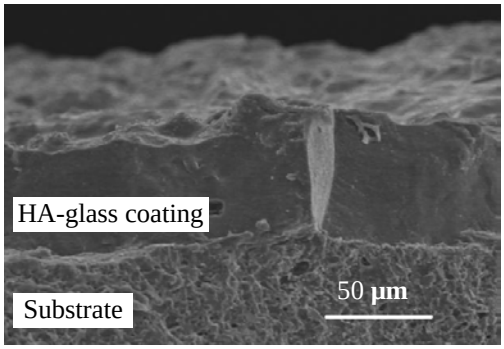

Figure.3 Micrograph of the coating

METHOD

X-ray Stress Measurement

The X-ray stress measurement is a method of obtaining surface stresses from calculations based on the change in lattice spacing of crystal. We set up the coordinate system as shown in Fig.1, σ_x is the stress in φ direction and ψ is the angle between the normal of diffraction plane and the normal of specimen surface. Based on this coordinate system, the relation between strains and stresses can be described as Eq. 1,

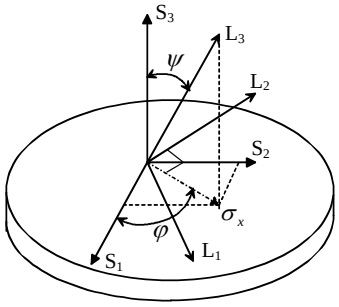

Figure.1 Coordinates of X-ray stress measurement

where σ_{11}, σ_{22} and σ_{33} are principal stresses.

$$\varepsilon_{33}^{L} = \frac{S_2}{2}(\sigma_{11}\cos^2\varphi + \sigma_{12}\sin 2\varphi + \sigma_{22}\sin^2\varphi)\sin^2\psi + \frac{S_2}{2}\sigma_{33}\cos^2\psi + S_1(\sigma_{11}+\sigma_{22}+\sigma_{33}) + \frac{S_2}{2}(\sigma_{13}\cos\varphi + \sigma_{23}\sin\varphi)\sin 2\psi \quad (1)$$

If we only consider the principal stresses and when φ=0,

$$\varepsilon_{33}^{L}=\frac{S_2}{2}(\sigma_{11}-\sigma_{33})\sin^2\psi+\frac{S_2}{2}\sigma_{33}+S_1(\sigma_{11}+\sigma_{22}+\sigma_{33}) \quad (2)$$

where ε_{33}^{L} can be deduced from Bragg's law as follows,

$$\varepsilon_{33}^{L}=-\frac{1}{2}\cot\theta_0(2\theta_\psi-2\theta_0) \quad (3)$$

Equating the Eq.2 and Eq.3, we obtain the following 2θ-$\sin^2\psi$ relation,

$$2\theta_\psi=-2\tan\theta_0\left\{\frac{S_2}{2}(\sigma_{11}-\sigma_{33})\sin^2\psi+\frac{S_2}{2}\sigma_{33}+S_1(\sigma_{11}+\sigma_{22}+\sigma_{33})\right\}+2\theta_0 \quad (4)$$

from Eq. 4, the stress $\sigma_{11}-\sigma_{33}$ is determined by the following equation;

$$\sigma_{11}-\sigma_{33}=-\frac{1}{S_2}\cdot\cot\theta_0\cdot\frac{\partial(2\theta_0)}{\partial(\sin^2\psi)}\cdot\frac{\pi}{180} \quad \text{(MPa)} \quad (5)$$

We name S_1 and S_2 as X-ray elastic constants (XEC) and they can be described as follows, E_x and ν_x are X-ray Young's modulus and Poisson's ratio.

$$S_1=-\frac{\nu_x}{E_x},\qquad S_2=\frac{2(1+\nu_x)}{E_x} \quad (6)$$

Defining K and M as

$$K=-\frac{1}{S_2}\cdot\cot\theta_0\cdot\frac{\pi}{180} \quad \text{(MPa/deg)} \quad (7)$$

$$M=\frac{\partial(2\theta_\psi)}{\partial(\sin^2\psi)} \quad (8)$$

where K is called stress constant and M is the slope of a linear line in the 2θ-$\sin^2\psi$ diagram.

Stress Estimation

In present study, X-ray diffraction was used to analysis the crystalline structures and determine the residual stresses in each coated layer. X-ray diffraction is a more suitable technique, with a better resolution for studying hydroxyapatite. (Millet, 2002) For the multiphase materials, X-ray diffraction technique is also proved to be an available method to estimate the micro stresses in each phase. As a consequence, influences of the graded structure on the internal stress distribution could be verified.

Hydroxyapatite is a ceramic and shows several different crystalline structures and amorphous phases. It affects the diffraction analysis with a multiplicity of diffraction peaks, frequently superimposed, that have low intensity on a high level background. (Millet, 2002) For a X-ray stress measurement, it is necessary to find an isolated peak with enough intensity and highest diffraction angle. In the case of HA, it is difficult to find an ideal isolated peak with high angle and high diffraction intensity. In our experiment, the (522) plane was used for the stress measurements. The (522) peak is in 139.3deg. and its diffraction intensity is high enough for the stress measurement. (Fig.4.) The detailed diffraction conditions used for the stress investigations are listed in Table 4. Elastic constants of HA were calculated using Kröner models. (Kröner, 1958) For the HA(522), $S_2/2=1.145\times10^{-5}$MPa^{-1} and $S_1=-0.261\times10^{-5}$MPa^{-1}.

Stress states of glass, especially when glass is one constituent phase in the composite material, however, could be hardly estimated by diffraction methods such as X-ray and neutron. Because glass is uncrystallized and an available diffraction peak for stress measurement could not be obtained. Considering this reason, the finite element method (FEM) was used in this study to predict the thermal residual stress distribution of the glass phase in the functionally graded coating.

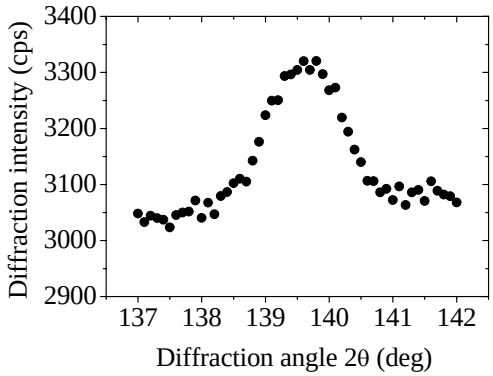

Figure.4 (522) peak used for stress measurement

Table 4. X-ray diffraction conditions

Diffraction plane, hkl	522
Diffraction angle, deg	139.3
Characteristic X-ray	Cr-Kα
Kβ-Filter	Cu
Tube voltage, kV	30
Tube current, mA	10
Radiation area, mm^2	4*6
Stress constant, MPa/deg.	-286.9
Measure method	Iso-inclination
Peak position	Half Value Breadth

Modeling Procedure for Computation Simulation

The computation simulations were done via OOF2, software which applies the finite element method at the microscale, by using microstructural images and materials properties as input data. (Langer, 2001,2006; Cannillo, 2006) OOF2 can calculate macroscopic properties from images of real or simulated microstructures, such as digitalized scanning electron microscope (SEM) pictures. It reads these images, assigns material properties to features in the image, and directly creates two-dimensional finite element meshes on them. Finally, the FEM solver conducts virtual experiments to determine the macroscopic properties of the microstructure.

In present work, distribution states of the constituent phases in each layer were observed from the SEM images that taken parallel to the coating surface. The distribution states of layers in the coating were observed through the SEM images for the coating cross section. OOF2 imported theses digitalized images, identified the constituent phases and assigned the correspondent material properties listed in Table 2. Finally, the finite element mesh was created. An example of the finite element mesh (Fig.5 (b)) that created from the SEM image (Fig.5 (a)) is shown, it contains about 4225 nodes and 4295 elements.

The residual stress that caused in the coating is because of the mismatch in the coefficient of thermal expansions between the coating and the substrate. It is assumed that the critical step is the cooling down after the sintering. For the graded coating structure in this work, no large mismatch in thermal expansion was caused between the Layer 1 and the substrate material because of their similar thermal property. From Layer2, with the increase of HA volume content, the residual stresses were generated in the coating because of the mismatch in the coefficient of thermal expansions between the HA phase and the glass phase. Considering the transition temperature of the glass used in this work is reported to be about 530^{o}C, (Borom, 1975) below the transition temperature the glass viscosity is so high that the thermal stresses

cannot be relaxed: a temperature decrease between the glass transition temperature and room temperature, ΔT =-510°C was decided.

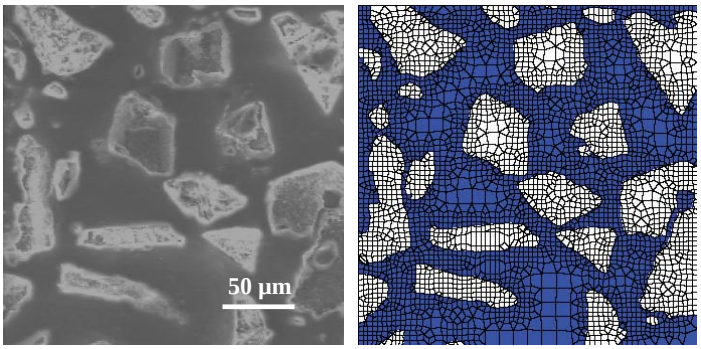

(a) SEM image (b) Created FEM mesh

Figure.5 Example of the FEM mesh that created from SEM image

RESULTS AND DISCUSSION

Experimental Measurement

In the experimental stress measurement, stress distributions of glass phase in the interlay could not be estimated by X-ray because of its uncrystallized property.

Fig.6 shows the measured residual stress distribution of HA phase in the coating: a gradual decrease in the residual stress values is observed as approaching the top layer (Layer6); tensile stresses are observed in the Layer4 and Layer5, compressive stress is observed in the top layer (Layer6). The measurement results also show the residual stress states for the HA phase in the coating with 150μm thickness are higher than those in the coating with 360μm thickness. Stress states of HA phase in the Layer1 to the Layer3 are not shown here, because the low volume fraction of HA phase in these layers induces large measurement errors.

Computational Simulation

Firstly, the plane thermal residual stress distributions are simulated via the SEM images parallel to the coating surface. Simulated stress distribution maps of the Layer4, the Layer5 and the Layer6 are shown in Fig.7. As expected, because of the difference in coefficient of thermal expansion between the HA and the glass, thermal residual stresses generated after the coating process. Since the coefficient of thermal expansion (12×10^{-6}°C^{-1}) of the HA is higher than that of the glass (10.4×10^{-6}°C^{-1}), the thermal residual stresses are mainly tensile in the HA and mainly compressive in the glass. The computational results of horizontal stress σ_{11} in each layer are summarized in Fig.8. Every result is the mean value of the calculations on five maps. Fig.8 shows a gradual decrease in the tensile stress for the HA, and a gradual increase in the compressive stress for the glass, as approaching the top layer (Layer6). This stress distribution behavior relates to the graded distribution of the constituent phases. In the Layer1, since no HA is used, no thermal residual stress is generated in the glass.

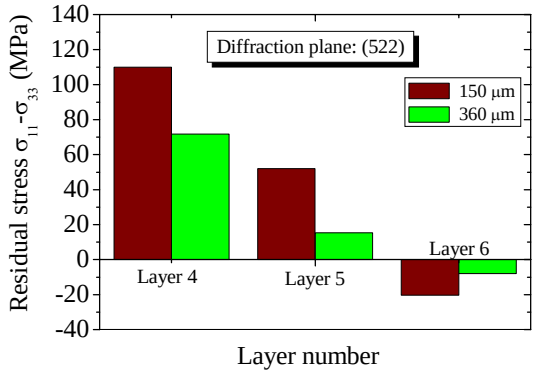

Figure.6 Experimental residual stresses distributions of HA phase in the coatings

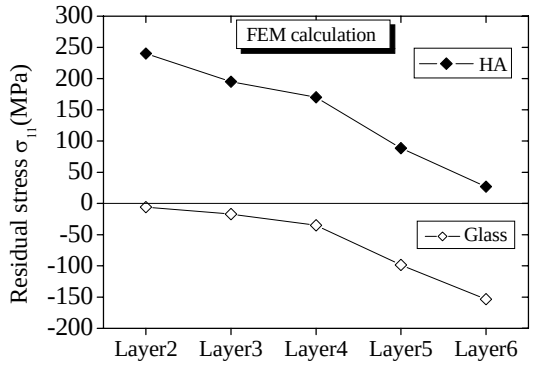

Figure.8 Computational residual stresses σ_{11} in the constituent phases

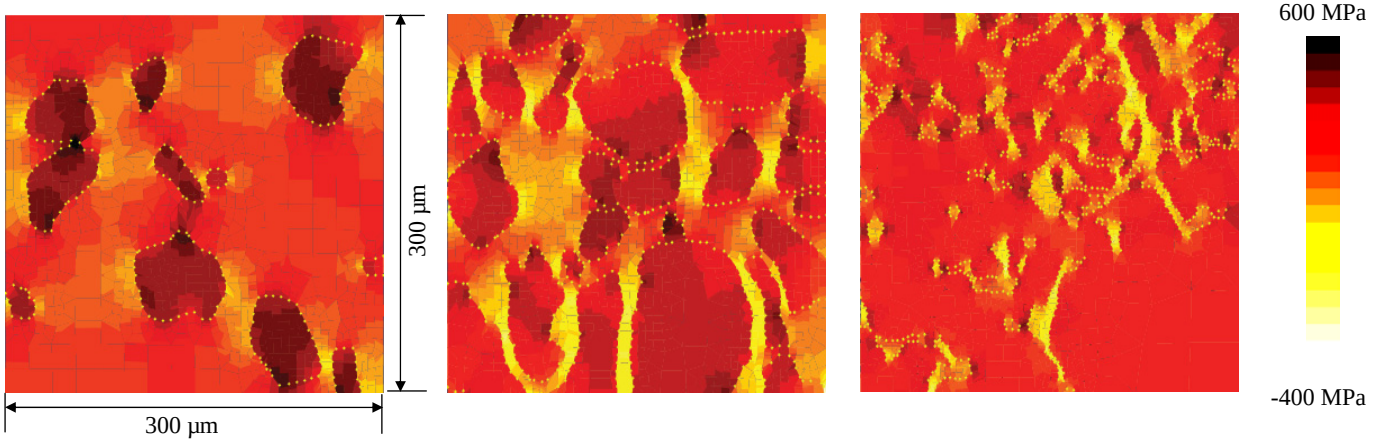

(a) Layer4 (b) Layer5 (c) Layer6

Figure.7 Simulated distributions of the horizontal stress σ_{11} in the inter-layers: the yellow points are used for distinguishing the interface of the HA and the glass

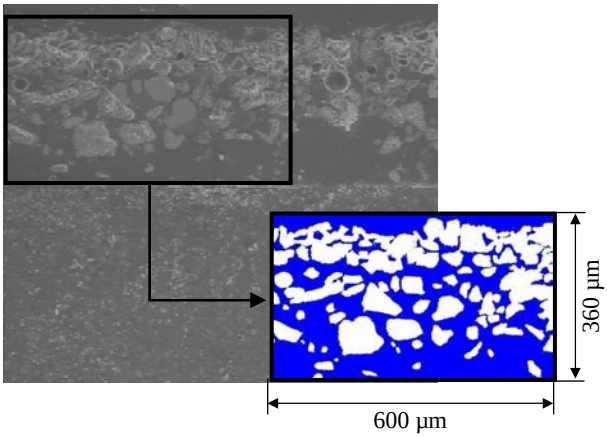

(a) Cross-section SEM micrograph and the preprocessed image used for calculation

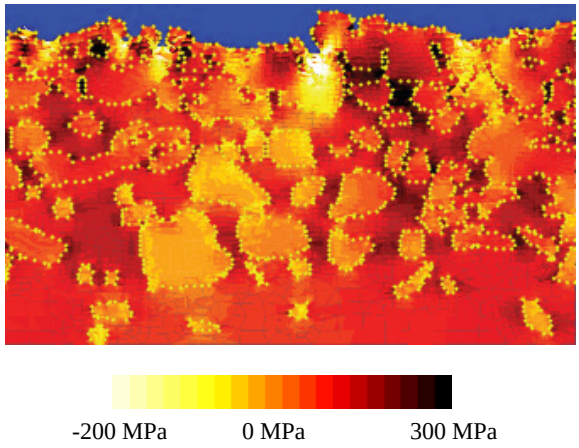

(b) Stress distribution map

Figure.9 Simulated distributions of the normal stress σ_{33} in the 360μm thickness coating: the yellow points are used for distinguishing the interface of the HA phase and the glass

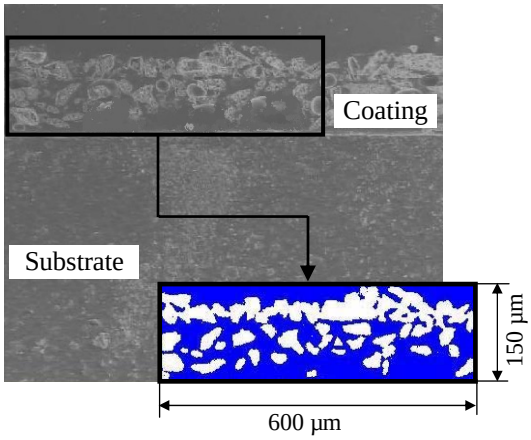

(a) Cross-section SEM micrograph and the preprocessed image used for calculation

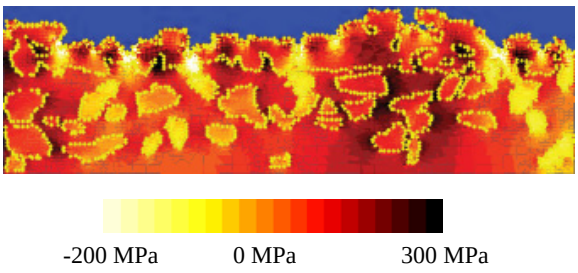

(b) Stress distribution map

Figure.10 Simulated distributions of the normal stress σ_{33} in the 150μm thickness coating: the yellow points are used for distinguishing the interface of the HA phase and the glass

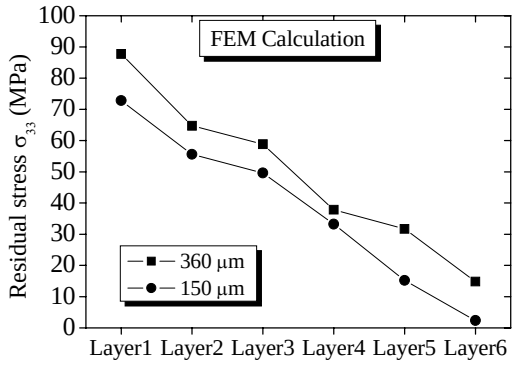

(a) HA phase

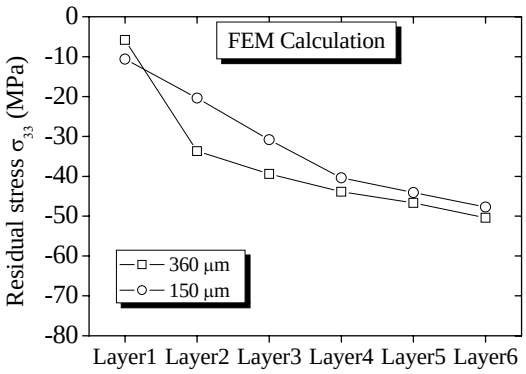

(b) Glass phase

Figure.11 Computational residual stresses σ_{33} in the constituent phases

Secondly, residual stress distributions in the cross-section of coating are investigated. Fig.9 (a) and Fig.10 (a) show the SEM images of the coating cross-section and the preprocessed images that used for the residual stress calculations in the 360μm and the 150μm thickness coatings, respectively. The spatial distribution of the constituent phases, the HA and the glass, are clarified. As the simulation results, Fig.9 (b) and Fig.10 (b) show the thermal residual stress distributions in the two coatings. We observe that, in both coatings, thermal residual stresses in the constituent phases show graded distribution behaviors. For the HA phase, the thermal residual stresses are tensile and increase gradually from the top layer to the bottom layer. For the glass phase, inversely, the thermal residual stresses are compressive and decrease gradually from the top layer to the bottom layer. Fig.11 shows the vertical normal

stress σ_{33} in the constituent phases that calculated from the stress distribution maps showed in the Fig.9 (b) and the Fig.10 (b). The results show the stress σ_{33} for the HA and the glass in the 360μm thickness coating are higher than those in the 150μm thickness coating.

As shown in the Table 3, the components of the corresponding layers in the two coatings are the same. We suggest that the HA volume fraction of one layer in the 150μm thickness coating is similar to that of the corresponding layer in the 360μm thickness coating. As a consequence, the plane thermal residual stress states of each layer in the two coatings are the same even though their thickness is different. As presented in Eq. 5, the experimental measured residual stresses showed in the Fig.6 are $\sigma_{11}-\sigma_{33}$ actually. To compare the experimental measured results with the computational calculated results, we have to make the comparison expressions coincide. According to the horizontal residual stresses σ_{11} showed in Fig.8 and the vertical normal residual stresses σ_{33} showed in Fig.11, we calculated the residual stresses $\sigma_{11}-\sigma_{33}$ in the constituent phases for the two coatings. (Fig.12) We observe the stress distribution behaviors of the HA phase are similar to those showed in the Fig.6: a gradual decrease in the residual stress values is observed as approaching the top layer (Layer6); the residual stress states in the 150μm thickness coating are higher than those in the 360μm thickness coating. In Fig.12, the stress distribution behaviors of the glass are also clarified: a gradual increase in the residual stress values is observed as approaching the top layer (Layer6); the residual stress states in the 150μm thickness coating are also higher than those in the 360μm thickness coating. In the Layer6, which mainly consists of HA, the tensile stress in the HA are under 30MPa; Below the Layer4, almost no residual stresses are induced in the glass phase, because of the low content of the HA. In the Layer1, calculation result show the residual stress is compressive and under 10MPa. It is because the coefficient of thermal expansion of the glass ($10.4\times10^{-6o}C^{-1}$) and the substrate material ($10\times10^{-6o}C^{-1}$) is about the same. These results are lower than the stress values reported by Tsui (1998), which is about 40MPa for Ti-6Al-4V substrate with plasma-sprayed HA coating. The calculations prove that the HA-glass compound graded structure can mitigate the residual stress between the top HA layer and the substrate material effectively.

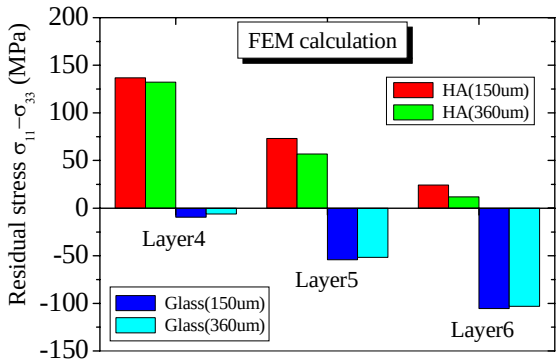

Figure.12 Computational residual stresses $\sigma_{11}-\sigma_{33}$ in the constituent phases

It should be noted, in the Layer6, stresses are experimentally measured to be compressive (Fig.6), but computationally observed ones are tensile (Fig.12). A reasonable explanation for this difference still cannot be given in this study. Two possible reasons are suggested. One is possibly because of the thermal expansion difference between the coating and the substrate. This difference maybe induces a bending deformation in the substrate in the cooling process. However, this influence is considered to be slight because thickness of the substrate is about 10 to 20 times the thickness of the coating, and it is not considered in the computation simulations. The other reason is maybe due to initial equipment error of the X-ray stress measurement. An equipment error about -25MPa was identified in the X-ray instrument.

CONCLUSIONS

(1) To improve the mechanical properties and eliminate the large residual stresses generated in the HA coating and the metal substrate, we successfully coated the HA-glass functionally graded materials on the ZTA ceramic substrate by means of Slurry-dripping and sintering method.

(2) This study focused on the estimation of the thermal residual stresses of the constituent phases in the coatings. The thermal residual stress states in the coatings are estimated by means of the experimental measurement and the FEM calculation, and the same thermal residual stress distribution behaviors are observed.

(3) The stress estimation results show: the graded compound HA-glass interlayer structure can mitigate internal stresses and control the density and kinetics of misfit emanating from interfaces effectively; the mitigate effect is more obvious with increasing thickness of the graded layers.

ACKNOWLEDGEMENT

The authors would like to thank Dr. Z.Q.Wang and his laboratory (Dalian Institute of Light Industry) sincerely for their contributive assistance in preparing specimens.

REFERENCES

Brown, Turner and Reiter et.al. (1994). "Residual Stress Measurement in Thermal Sprayed Hydroxyapatite Coatings," *J Mater Sci: Mater Med*, Vol 5, pp 756-759.

Berndt, Haddad and Farmer (1990). "Thermal Spraying for Bioceramic Applications", *Mater Forum*, Vol 14, pp161-173.

Borom, Anna and Turkalo et.al (1975). "Strength and Microstructure in Lithium Disilicate Glass-Ceramics," *J Am Ceram Soc*, Vol 58, No 9-10, pp 385-391.

Cannillo, Montorsi and Siligardi et.al (2006). "Microscale Computational Simulation and Experimental Measurement of Thermal Residual Stresses in Glass-alumina Functionally Graded Materials," *J Eur Ceram Soc*, Vol 26, pp 1411-1419.

Che, Gotoh and Lin et.al (2007). "Residual Stress State of Hydroxyapatite Graded coating on Ceramic Substrate," *Adv X-ray Ana*, (In press)

Holmes, Bucholz and Monney (1986). "Residual Stress Measurement in Thermal Sprayed Hydroxyapatite Coatings," *J Bone Surg*, Vol 68(A), pp 904-911.

Geesink, Groot, and Klein (1987). "Bonding of Bone to Apatite-coated Implants," *Clin Orthop*, Vol 225, pp 147-170.

Grenoble, Katz and Dunn et.al (1972). "The elastic properties of hard tissues and apatites," *J Biomed Mat Res*, Vol 6, No 3, pp 221-223.

Klein, Patsa and Wolke et.al (1994). "Long-term in vivo Study of Plasma-sprayed Coatings on Titanium alloys of Tetra-caicium Phosphate, Hydroxyapatite and α—tricalcium Phosphate," *Biomaterials*, 15, pp 146-150.

Kröner (1958). "Berechnung der elastischen Konstanten des Vielkristalls aus den Konstanten des Einkristalls," *Ergebn Angew Math*, Vol 5, pp 504.

Li, Lee and Kobayashi et.al (1996). "Hydroxyapatite Coating by Dripping Method, and Bone Bonding Strength," *J Mater Sc: Mater Med*, Vol 7, pp 355-357.

Lacefield (1988). "Hydroxyapatite Coating," *Ann NY Acad Sci*, Vol 523, pp 72-80.

Langer, Fuller and Carter (2001). "OOF: An Image Based Finite-element Analysis of Material Microstructures," *Comput Sci Eng*, Vol 3, No 3, pp 15-23.

Langer, Reid and Haan et.al (2006). "The OOF2 Manual, Version 2.0".

Miyamoto, Kaysser and Rabin et.al. (1999). "Functionally Graded Materials. Design, Processing and Application," Kluwer Academic Publishers.

Millet, Girardin and Braham et.al (2002). "Stress Influences on Interface in Plasma-sprayed Hydroxyapatite Coatings on Titanium Alloy," *J Biomed Mater Res*, Vol 60, pp 679-684.

Ong and Lucas (1994). "Post-deposition Heat Treatment for Ion Beam Sputter Deposited Calcium Phosphate Coatings," *Biomaterials*, Vol 15, pp 337-341.

Rao, Iwasa and Tanaka et.al (2003). "Preparation and Mechanical Properties of Al_2O_3-15 wt.%ZrO_2 Composites", *Scri. Mater.*, Vol 48, pp 437-441.

Tsui, Doyle and Clyne et.al (1998). "Plasma Sprayed Hydroxyapatite Coatings on Titanium Substrates. Part I. Mechanical Properties and Residual Stress Levels", *Biomaterials*, Vol 19, pp 2015-2029.

Wang, Lee and Chang et.al (1993). "The Shear Strength and the Failure Mode of Plasma-sprayed Hydroxyapatite Coating to Bone," *J Biomed Mater Res*, Vol 27, pp 1315-1327.

Wang, Chen and Cai et.al (2003). "Influences of R_2O-Al_2O_3-B_2O_3-SiO_2 System Glass on the Sintering and Phase Transition of Hydroxyapatite," *Glass & Enamel*, Vol 31, No 1, pp 16-19.

Yang, Chang and Hwang et.al (2000). "Biaxial Residual Stress States of Plasma-sprayed Hydroxyapatite Coatings on Titanium Alloy Substrate," *Biomaterials*, Vol 21, pp 1327-1337.